applied sciences

MDPI

Article

Analysis of Adaptive Fractional-Order Sliding-Mode Control Method Based on Smith Predictor for Voice Coil Motor

Ziyi Shi and Xiaobao Yang *

College of Electrical Engineering, Sichuan University, Chengdu 610065, China
* Correspondence: yang_xb@scu.edu.cn; Tel.: +86-028-8540-5111

Abstract

To satisfy the stringent requirements of ultra-precision systems for high accuracy and rapid dynamic response, the chatter and system delay of voice coil motor (VCM) under operating conditions have become key bottlenecks restricting overall performance enhancement. To address these challenges, this paper proposes an adaptive convergence rate fractional-order sliding mode control strategy based on a Smith predictor (AFOSMC-SP). The strategy constructs a fractional-order sliding mode controller using an improved Oustaloup method, introduces a novel adaptive reaching law based on a saturation function with dynamic gain, and integrates a Smith predictor to compensate for the current-loop delay in the VCM system. This approach reduces algorithmic complexity and position-tracking error while enabling the adaptive adjustment of the system convergence rate to enhance robustness. In addition, the parameter boundary conditions and the global asymptotic stability of the closed-loop system are analyzed using Lyapunov stability theory. The simulation results show that, compared to conventional sliding mode control methods, the proposed AFOSMC-SP strategy provides superior parameter adaptability, higher tracking accuracy, and stronger suppression of external disturbances.

Keywords: voice coil motors; adaptive fractional-order; sliding mode control; smith predictor

1. Introduction

As integrated circuit technology continuously pursues higher-level upgrades, the performance requirements for ultra-precision workbenches have reached unprecedented heights. In this context, voice coil motors, as the power source for high-end equipment such as lithography machines, play an increasingly prominent role and have become one of the key factors driving technological advancement [1–3]. Compared with traditional motion platforms that rely on the piezoelectric effect, voice coil motors do not require complex mechanical transmission mechanisms in their structural design, offering advantages such as large travel, fast response, strong load capacity, and the ability to maintain high precision and stability under various working conditions [4]. However, due to their direct-drive nature, voice coil motors are prone to being affected by environmental disturbances and system nonlinearities in actual operation, posing control challenges.

With the continuous development of control theory, sliding mode control (SMC) has been widely applied to high-performance systems due to its strong robustness against system uncertainties, parameter variations, and external disturbances, as well as its excellent tracking accuracy and fast response. However, during the switching process of SMC, the system state points repeatedly cross the sliding surface, causing noticeable chattering and

Check for updates

Academic Editor: Gerard Ghibaudo

Received: 27 November 2025
Revised: 31 December 2025
Accepted: 5 January 2026
Published: 7 January 2026

Copyright: © 2026 by the authors. Licensee MDPI, Basel, Switzerland. This article is an open access article distributed under the terms and conditions of the Creative Commons Attribution (CC BY) license.

leading to performance degradation. To achieve accelerated convergence and suppress chattering, reference [5] introduced system state variables and exponential functions based on the traditional exponential reaching law, which effectively reduces chattering while ensuring fast convergence and robustness. However, this method involves six parameters that need to be tuned, making the design complex. Reference [6] proposed a method combining adaptive fuzzy control with super-twisting sliding mode, which can effectively handle time-varying disturbances. Some quasi-smooth methods [7,8] and high-order smoothing methods [9,10] can reduce chattering to some extent, but they still face limitations such as degraded control performance [11], incomplete chattering suppression [12], or poor transient response [13]. Fractional-order sliding mode control (FOSMC) provides an effective solution to these problems. By introducing a fractional-order sliding surface, FOSMC can attenuate high-frequency chattering during switching by gradually dissipating energy, thereby effectively suppressing control vibrations [14]. Reference [15] used a dead-zone hysteresis function to reduce the switching frequency, thus decreasing the chattering amplitude, but the steady-state error problem remains unsolved. Reference [16] introduced a PI-type FOSMC to enhance the system's dynamic performance and disturbance rejection ability. Reference [17] used a saturation function instead of a sign function to mitigate chattering. Reference [18] proposed an AFOSMC method based on a nonlinear disturbance observer, which showed remarkable effects, but had limited applicability. Reference [19] introduced fuzzy fractional-order sliding mode control to improve system tracking accuracy, while reference [20] significantly enhanced the system's transient response using a fractional-order integral terminal sliding mode control strategy.

Although existing FOSMC methods have made certain progress, the above literature does not fully consider the influence of the approaching rate on chattering suppression and overall control performance. Meanwhile, current approaches also fail to account for the sampling delay commonly present in high-precision voice-coil-motor (VCM) control. Even a very small delay may prevent the system from responding to disturbances in time, resulting in large overshoot and longer settling time [21]. In motor-control systems and related fields, the Smith predictor has been proven effective for compensating pure time delays. For a given signal, the Smith predictor can estimate the post-disturbance system dynamics in advance and compensate for delay-induced errors, thereby reducing overshoot and shortening the settling time [22]. As part of a composite control strategy, Ref. [23] combined a Smith predictor with a fractional-order PID controller to enhance tracking performance and disturbance rejection. However, when the load varies or the system was affected by external disturbances and time delays, traditional PID control and the fixed-gain approaching rate of sliding mode control cannot meet the requirements of high dynamic response and stability in ultra-precision stages. Therefore, the core problem addressed in this paper is to mitigate the chattering and time-delay issues of the VCM under operating conditions. To achieve high responsiveness and low delay, an adaptive approaching-rate fractional-order sliding mode control method is adopted and integrated with a well-established Smith predictor.

To this end, this paper proposes an AFOSMC strategy based on the Smith predictor. By designing a fractional-order integral function, employing the modified Oustaloup method, and introducing an adaptive approaching rate, the proposed approach effectively overcomes the chattering problem in conventional SMC strategies and enhances the robustness and tracking accuracy of the control system. Meanwhile, by incorporating the Smith predictor, the method significantly reduces the time delay introduced by the current loop of the VCM.

The rest of the paper is organized as follows. Firstly, the mathematical model of voice coil motor is given, and the Smith predictor is designed to reduce the time delay in the

current loop. Meanwhile, a FOSMC strategy based on a novel adaptive convergence rate is proposed. Section 3 designs the improved fractional-order algorithm and the adaptive approaching rate, and ultimately develops a FOSMC controller for the voice-coil motor to reduce chattering. In Section 4, a Lyapunov stability analysis is carried out to ensure the reliability of the control strategy. Section 5 discusses the simulation results. Finally, Section 6 contains our concluding remarks and ideas for future work.

2. Mechanical and Electrical Mathematical Models of the Voice Coil Motor

A moving coil-type external magnetic voice coil motor, as shown in Figure 1, is selected in this paper, and the mathematical model of its actuator is established. Let the voltage of the drive motor be of magnitude U, the equivalent resistance and inductance of the motor coil winding be R_a and L_a, respectively, and the mass of the actuator be m. The current through the coil conductor be I, and the magnitude of the resulting counter electromotive force be E_a. The relevant parameter values are listed in Table 1.

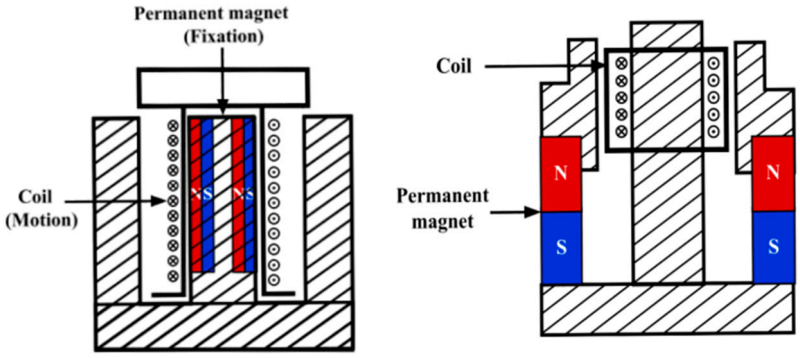


Figure 1. Schematic diagram of moving coil type voice coil motor structure.

Table 1. Performance parameters of voice coil motor.

Parameter Name	Symbol	Unit	Value
Ampere force constant	K	(N/A)	12.7
Back electromotive force constant	K_e	V/(m/s)	12.7
Interphase resistance	R_a	Ω	5
Interphase inductance	L_a	mH	1
Electromagnetic time constant	T_a	ms	0.2
Weight of the moving object	m	g	45
Outside diameter	C	mm	40
Height	H	mm	39.9
Peak thrust	F_p	N	80
Maximum winding temperature	T_{max}	°C	150
Current loop feedback coefficient	K_c		1
Sampling filter time	T_c	ms	0.1
Amplification coefficient of motor current closed-loop modulation stage	K_{pwm}		2.4

The voltage balance equation is established according to Kirchhoff's voltage law: $U_\infty = R_a I + E_a = R_a I + BLv$. In order to control the moving part of the voice coil motor to carry out different degrees of back and forth motion, its coil current varies continuously. During this process, the equivalent inductance of the coil produces a certain voltage drop: $U_L = L_a \frac{dI}{dt}$. It is possible to formulate the voltage balance equation:

$$U = U_\infty + U_L = R_a I + BLv + L_a \frac{dI}{dt} \tag{1}$$

Considering the part of the acceleration produced by the electromagnetic force during the acceleration of the coil, denoted as f_a, one obtains (2):

$$f_a = ma = m\frac{dv}{dt} = m\frac{d^2x}{dt^2} \tag{2}$$

The resistance generated by the motor in the process of movement is uniformly equivalent to the damping force that is proportional to the linear velocity of the coil, and its coefficient corresponding to the generation of the damping effect is also co-equivalent counted as K_f, and the size of its resistance is

$$F_f = K_f v = K_f \frac{dx}{dt} \tag{3}$$

When the actuator is working, it is subjected to the effects of current and resistance, resulting in acceleration. Then the force balance equation of the voice coil motor can be derived, and the expression for the current in the coil can be obtained:

$$I = \frac{m}{k}\frac{d^2x}{dt^2} + \frac{K_f}{K}\frac{dx}{dt} \tag{4}$$

The expression for the input voltage U of the motor with respect to the linear displacement x of the actuator is obtained by eliminating the variable I by association:

$$U = \frac{L_a m}{K}\frac{d^3x}{dt^3} + \frac{R_a m + L_a K_f}{K}\frac{d^2x}{dt^2} + \frac{R_a K_f + K_c K}{K}\frac{dx}{dt} \tag{5}$$

The relationship between the motor coil voltage and the actuator displacement in the complex frequency domain is obtained after performing the Laplace transform and disassembling and reorganizing. This equation is able to show the expression of the transfer function of the control input voltage to the motor output displacement:

$$\frac{X(s)}{U(S)} = \frac{1}{s}\frac{K\frac{\frac{1}{ms}}{(1+K_f\frac{1}{ms})}\frac{1}{(L_a s+R_a)}}{1+K_c[K\frac{\frac{1}{ms}}{(1+K_f\frac{1}{ms})}\frac{1}{(L_a s+R_a)}]} \tag{6}$$

According to the closed-loop transfer function and open-loop transfer function, the calculation formulas can be correspondingly introduced voice coil motor's mathematical model of the mechanical feedback loop and electrical feedback loop of the open-loop transfer function expressions, as shown in (7) and (8).

$$G_F(s) = \frac{1}{ms} \tag{7}$$

$$G_E(s) = K\frac{\frac{1}{ms}}{(1+K_f\frac{1}{ms})}\frac{1}{(L_a s+R_a)} \tag{8}$$

Meanwhile, considering the delay generated by sampling and filtering during the operation of the motor, a Smith predictor is introduced on the basis of the motor current negative feedback to compensate for the delay, further offsetting the time lag caused by the current loop and improving its dynamic response, and Equation (9) is the expression of the predictor transfer function:

$$G_c = \frac{K_c K_{pwm}}{R_a T_c s^2 + R_a s + K_c K_{ci}} e^{-\tau s} \tag{9}$$

K_c is the current feedback coefficient, T_c is the current sampling time constant, K_{pwm} is the pulse width modulation amplification coefficient, the integration time coefficient of the current loop regulator is K_c, and $e^{-\tau s}$ is the delay in the sampling and transmission process of the motor system.

3. Design of FOSMC for Voice Coil Motor

3.1. Improved Oustaloup Algorithm Parameter Design

This paper selects Caputo fractional calculus (its specific form is shown in the Appendix A) and uses an improved Oustaloup method to solve the numerical solution of the fractional-order controller transfer function. This method provides higher approximation accuracy at the frequency band endpoints, can decompose fractional-order differential equations into a series of transfer functions, and, combined with conventional controller design methods, obtains the numerical solution.

The improved Oustaloup method enhances approximation accuracy by introducing parameters b and d. These parameters slightly extend the fitting frequency band and redistribute the pole-zero pairs, yielding the new approximation expression (10):

$$s^p \approx \left(\frac{d\omega_1}{b}\right)^p \left(\frac{ds^2 + b\omega_h s}{d(1-p)s^2 + b\omega_h s + d\alpha}\right) \prod_{k=-N}^{N} \frac{s + \omega_k'}{s + \omega_k} \tag{10}$$

Among them, the real zero pole can also be written as shown in (11) and (12).

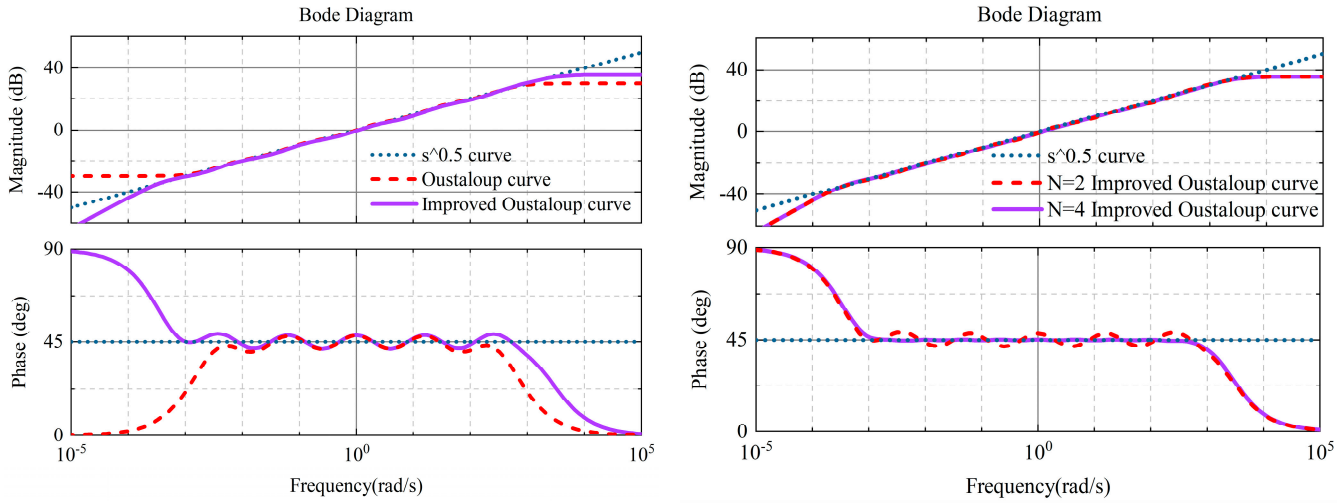
$$\omega_k = \left(\frac{d\omega_h}{b}\right)^{\frac{p+2k}{2N+1}} \tag{11}$$

$$\omega_k{}' = \left(\frac{d\omega_1}{b}\right)^{\frac{p-2k}{2N+1}} \tag{12}$$

Then let the constant parameter in the improved computational expression be satisfied: $\beta = \frac{d}{b} > 0$. Simplifying (10) will give the transfer function of the fractional-order operator s^{p} with respect to the two main parameters p and β derived from the improved Oustaloup filter approximation method, as shown in (13). Generally, b = 10 and d = 9 are taken. This reduces the approximation error near ω_{L} and ω_{H} while preserving the stability of the approximated operator.

$$G_p(s) = \beta^p {\omega_b}^p \frac{\beta s^2 + \omega_h s}{(1-p)\beta s^2 + \omega_h s + p\beta} \prod_{k=-N}^{N} \frac{s + \omega_k'}{s + \omega_k} \tag{13}$$

The equivalent integer order transfer function is obtained by approximate fitting in the target frequency band [0.001, 1000] using the improved Oustaloup method approach for the 0.5 order differential operator $s^{0.5}$. By fitting with order $2N + 1 = 5$, i.e., $N = 2$, the transfer function shown in the Bird plot in Figure 2a is obtained, and the improved Oustaloup method for this fractional-order differentiation has better accuracy in fitting at the two ends of the target frequency band and a wider range of bands approximated to coincide with the actual curves, which is indeed superior to that of the traditional algorithm. By further increasing the approximation order to 2N + 1 = 9, as shown in Figure 2b, it can be observed that within a certain frequency range, a higher order reduces frequency-domain fluctuations, thereby improving the approximation accuracy. Table 2 lists the pole and zero frequencies of the system for N = 2 and N = 4, illustrating the influence of the approximation order on the model structure. In the process of actual design parameters, in order to achieve better approximation accuracy of fractional-order operator, and considering the complexity of the calculation, it is recommended to choose the filter order parameter N = 2~4. Using the above design procedure, the poles and zeros of the modified Oustaloup approximation for p = 0.5 with N = 2 and N = 4 are calculated and listed in Table 2.



(**a**) (**b**)

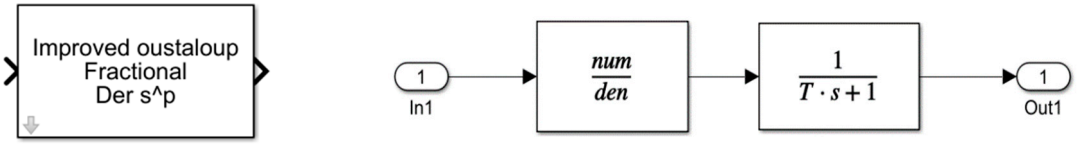
Figure 2. (**a**) Bode plots of the results of fitting the Oustaloup method to the fractional-order differential operator $s^{0.5}$ before and after the improvement. (**b**) Bode plots of the effect of the improved Oustaloup method for fitting $s^{0.5}$ at different values of N.

Table 2. Zero frequencies and pole frequencies at N = 2 and 4.

Parameter	N	K	Zero Frequency	Pole Frequency
P = 0.5	2	1	5.477226×10^{-5}	1.778279×10^{-7}
		2	4.929503×10^{-10}	1.778279×10^{-12}
	4	1	2.340347×10^{-4}	1.333521×10^{-5}
		2	7.021042×10^{-7}	4.216965×10^{-8}
		3	2.106313×10^{-9}	1.333521×10^{-10}
		4	6.318938×10^{-12}	4.216965×10^{-13}

During the approximation process, the improved Oustaloup algorithm may result in the numerator and denominator having the same order. In Simulink, this situation can lead to algebraic loops, which may cause simulation delays, oscillations, or even simulation failure.

To avoid this issue, a low-pass filter with a bandwidth of ω_l is cascaded after the fractional-order operator module to break the algebraic loop, thereby rendering the system strictly causal and ensuring simulation accuracy and stability. The encapsulated module of the improved Oustaloup filter method is shown in Figure 3a, and its internal structure is shown in Figure 3b.



(**a**) (**b**)

Figure 3. Encapsulated module of the improved Oustaloup filter method and its internal structure.

3.2. Adaptive Fractional-Order Sliding Mode Convergence Rate Design

In the design of FOSMC, nonlinear sliding mode surfaces are involved in the system state space. To simplify the calculations, this design selects a linear sliding surface as the

switching surface, directly incorporating the Caputo defined fractional calculus operator ${}_{a}D_{t}{}^{-p}$ into the equation of this linear switching surface to obtain Equation (14). Then, by performing fractional-order differentiation on both sides of the equation, the fractional-order sliding mode switching surface in the form of Equation (15) is obtained:

$$s = c_1 x_1 + c_2 \, {}_a D_t^{\alpha} x_2 \quad 0 < \alpha < 1 \tag{14}$$

$$\dot{s} = c_1 \dot{x}_1 + c_2 \, {}_a D_t^{\alpha+1} x_2 \tag{15}$$

In a fractional-order sliding mode controller, the sign function sgn(s) can achieve the control objective. However, the high-frequency switching of sgn(s) near the origin can cause high-frequency jumps in the control input signal, which adversely affects the system's stability and control accuracy. To address this issue, this study adopts a quasi-sliding mode approach and introduces the concept of a 'boundary layer,' replacing the sign function with the saturation function sat(s), as shown in Equation (16):

$$sat(s) = \begin{cases} \operatorname{sgn}(s) & |s| \geq \Delta \\ \frac{s}{\Delta} & |s| < \Delta \end{cases} \tag{16}$$

where Δ is the thickness of the boundary layer. When the system state is located outside the boundary layer, the saturation function has the same effect as the sign function; when the system state enters the boundary layer region, the saturation function makes the control input change continuously, avoiding the sudden change in behavior, and then eliminating the high-frequency chatter vibration phenomenon. As the saturation function boundary layer has a more moderate transition process, the strong chatter generated by the symbol function switching is eliminated, resulting in a smoother following convergence effect of the system.

In order to further improve the convergence performance of the system, it is usually necessary to consider both chattering issues and convergence speed when designing the convergence rate. To address the limitations of the traditional exponential convergence law, this paper proposes a new adaptive convergence rate and, by combining the advantages of the saturation function, obtains a fractional-order approaching rate using Equation (17):

$$\begin{aligned} & D_t^{\beta} s = -\varepsilon f(s) sat(s) - ks, \varepsilon > 0, k > 0 \\ & \begin{cases} f(s) = \frac{1}{1+e^{-s}} \\ k = k_0 + k_1 \cdot e^{-\gamma |s|} \end{cases} \end{aligned} \tag{17}$$

where k_0 is a fixed gain, k_1 is a variable gain used to adjust the dynamic gain amplitude, γ controls the exponential decay rate (the larger its value is, the more the gain tends to be stabilized), and $f(s)$ is a sigmoid function. The convergence rate is adaptively adjusted according to the size of the sliding mode variable s. When s is larger, the control gain is higher and the system exerts a stronger control force to ensure that the state converges quickly to the slip mode surface, thus accelerating the convergence rate. When s is small, the control gain gradually decreases, and the system control strength is weakened to avoid the high-frequency chatter phenomenon due to too-fast convergence.

Differentiating the expression (17) yields the fractional-order sliding mode convergence law ultimately adopted.

$$\dot{s} = D_t^{1-\beta} [-\varepsilon f(s) sat(s) - ks] \tag{18}$$

3.3. Fractional-Order Sliding Mode Controller Strategy Based on Voice Coil Motor

In order to improve the dynamic performance of the speed closed-loop, this paper designs a fractional-order sliding mode controller for its optimization and establishes the

state-space expression of the speed loop. By selecting speed as the control state variable, the state-space expression related to the current can be obtained, as shown in Equation (19). Where v_d is the velocity value of the given input, v is the feedback value of the velocity loop, x_1 and x_2 correspond to the deviation of the velocity and its derivative.

$$\begin{cases} \dot{x}_1 = -\frac{dv}{dt} = -a = -\frac{BL}{m}i = x_2 \\ \dot{x}_2 = -\frac{d^2v}{dt^2} = -\frac{BL}{m}i' \end{cases} \tag{19}$$

Again, let $u = \frac{di}{dt}$ and $M = \frac{BL}{m}$ hold and rewrite the expression in matrix form, as shown in (20).

$$\begin{bmatrix} \dot{x}_1 \\ \dot{x}_2 \end{bmatrix} = \begin{bmatrix} 0 & 1 \\ 0 & 0 \end{bmatrix} \begin{bmatrix} x_1 \\ x_2 \end{bmatrix} + \begin{bmatrix} 0 \\ -M \end{bmatrix} u \tag{20}$$

Based on the state-space expression of the voice coil motor and the fractional-order linear sliding mode surface selected in Section 3.2, and using Equation (18) for discretization, the derivative expression of the state variable x_2 with respect to the control input u can be obtained (21):

$$\dot{x}_2 = -Mu = D_t^{1-\alpha-\beta}[-\varepsilon f(s)sat(s) - ks] - D_t^{-\alpha}c_2x_2 \tag{21}$$

In the above equations, the values of α and β are in the range (0, 1). From (21), the control equation can be solved for the control variable:

$$u = -\frac{1}{M}D_t^{1-\alpha-\beta}[-\varepsilon f(s)sat(s) - ks] - \frac{1}{M}D_t^{-\alpha}c_2x_2 \tag{22}$$

Integrating (22) yields the final expression for the coil current under the fractional-order sliding mode control strategy (23):

$$i = \frac{1}{M}\int_0^t \left\{ D_t^{1-\alpha-\beta}[\varepsilon f(s)sat(s) + ks] + D_t^{-\alpha}c_2x_2 \right\} d\tau \tag{23}$$

4. Stability Analysis of AFOSMC-SP System for Voice Coil Motor

The core idea of the Smith predictor design in this paper is to predict the future output of the system using a delay-free model, thereby compensating for the fixed delay introduced by sampling and computation in the control loop. In this study, since the controlled plant is a linearly modelable VCM current loop and the delay source is single and can be equivalently regarded as a fixed transmission delay, the classical Smith predictor structure is adopted. After delay compensation, the controller is effectively dealing with a delay-free system; therefore, the tuning of the sliding mode parameters only needs to be based on the delay-free model. Under this condition, the employed Smith predictor is stable and does not affect the overall system stability.

To ensure that the system states can enter the vicinity of the sliding surface within finite time and maintain smooth sliding motion after reaching it, a fractional-order reaching law under the Caputo definition is adopted in Equation (18). To verify the convergence of the proposed reaching law, the Lyapunov direct method is employed to analyze the stability of the sliding variable. According to the commonly used formulation of the fractional-order Lyapunov criterion, stability can be determined by selecting a positive definite scalar function $V(t)$ and examining the sign of its fractional-order derivative of order $p \in (0, 1]$. Accordingly, let

$$V(t) = \frac{1}{2}s^2 \tag{24}$$

Taking its derivative and substituting the designed fractional-order reaching law yields Equation (25).

$$\dot{V}(t) = s\dot{s} = sD_t^{1-\beta}[-\varepsilon f(s)sat(s) - ks] \quad (25)$$

Since $D_t^{1-\beta} > 0$, $k > 0$, $\varepsilon \geq 0$, $f(s) \geq 0$, and $s \cdot \mathrm{sat}(s) \geq 0$, Equation (26) can be obtained.

$$V(s) = -sD_t^{1-\beta}\varepsilon f(s)sat(s) - kD_t^{1-\beta}s^2 \leq -kD_t^{1-\beta}s^2 \quad (26)$$

The right-hand side is a positive definite function with respect to s; therefore, the negative definiteness condition required by the fractional-order Lyapunov theorem is satisfied. Consequently, the equilibrium point $s = 0$ is Mittag–Leffler asymptotically stable.

The existence of sliding mode motion is generally guaranteed by two conditions: reachability and invariance. From Equation (26), since V(s) = 0 if and only if $s = 0$, the system trajectories can reach the sliding surface $s = 0$. Substituting $s = 0$ into Equation (25) yields $\dot{s} = 0$, indicating that the system trajectories remain on the sliding surface once they reach it. Hence, the invariance of the sliding surface is ensured.

5. System Simulation and Results Analysis

5.1. Analysis of Simulation Results of AFOSMC-SP System

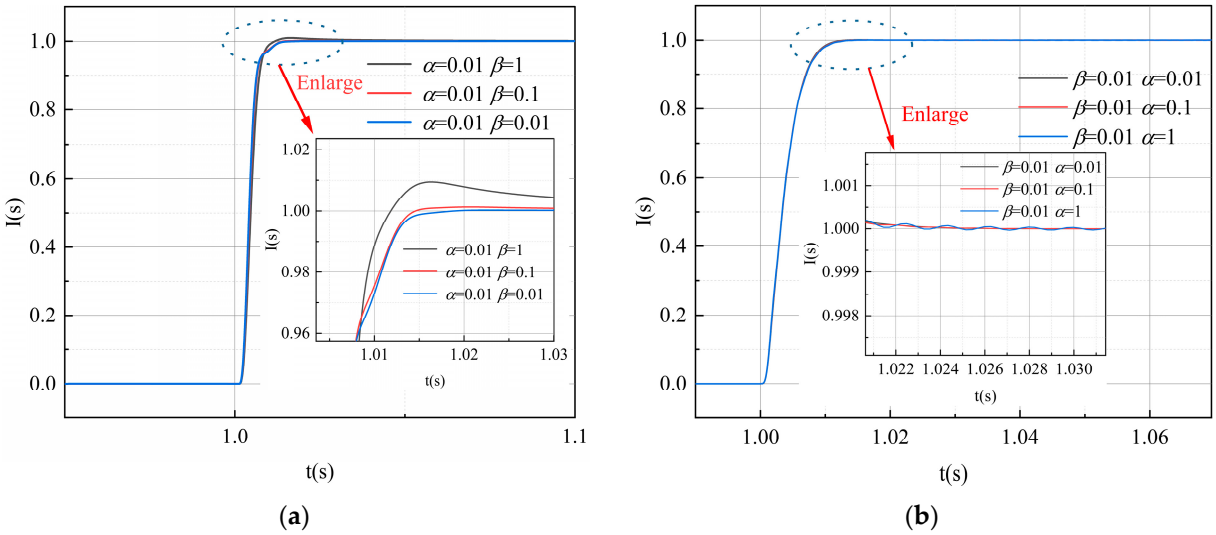
After the derivation of the AFOSMC equation is completed, it is applied to the voice coil motor control system to construct a speed loop AFOSMC-SP simulation model. The parameters to be tuned mainly include Oustaloup approximation-related parameters and sliding mode controller parameters. The control variable method is used to analyze the impact of each parameter on system performance one by one, providing a basis for system parameter selection.

The parameters of the sliding mode controller are set to $c_1 = 105$, $c_2 = 0.1$, and $\varepsilon = 105$. The modified Oustaloup filter method is used and the order 2N + 1 is selected. $\alpha = 0.1$ is set and β is adjusted, and the response curve of the system to the step function is shown in Figure 4a. The results show that the appropriate adjustment of the order β of the reduced convergence law can reduce the output overshoot and shorten the regulation time into the error band. Accordingly, setting $\beta = 0.1$ and adjusting α, the system step response curve is shown in Figure 4b. It is observed that the curve fluctuation and the change rule of β are similar, and too large of an α may lead to the degradation of the dynamic performance of the system. Meanwhile, in practical systems, the selection ranges of the parameters α and β are constrained within 0 to 2 [24]. Therefore, in order to reduce the overshooting of the response curve and improve the dynamic performance, it is recommended to select smaller α and β. In the simulation of the proposed the AFOSMC-SP strategy for the voice coil motor, $\alpha = 0.01$, $\beta = 0.01$, and $1 - \alpha - \beta = 0.98$ are selected as the parameters of the fractional-order operator. Tables 3 and 4 present a comparison of the system dynamic performance under different values of α and β.

Next, the influence of the filter order parameter N is investigated. In theory, increasing the filter order improves the approximation accuracy of the modified Oustaloup algorithm. However, comparative tuning results indicate that further increasing the filter order of ${}_aD_t^{-1-\alpha-\beta}$ only leads to marginal reductions in overshoot and settling time. Therefore, the filter orders are set to $N_{1-\alpha-\beta} = 4$ for ${}_aD_t^{-1-\alpha-\beta}$ and $N_\alpha = N_{-\alpha} = 4$ for ${}_aD_t^{\alpha}$ and ${}_aD_t^{-\alpha}$.

Meanwhile, the effects of parameters c_1 and c_2 on the system dynamic performance under different values are further analyzed. Both parameters are positive design coefficients used to balance the weighting between the state variable term and the fractional-order dynamic term in the sliding surface, where c_1 mainly influences the system response speed, while c_2 determines the contribution of the fractional-order term to dynamic smoothness. With $\varepsilon = 50$, the system responses are evaluated by varying $c_2 = 20$ and $c_1 = 50$, as shown in Figure 5. The results indicate that increasing c_1 shortens the settling time but increases

overshoot, while reducing c_2 helps improve the settling performance. Tables 5 and 6 summarize the dynamic performance under different values of c_1 and c_2.



(**a**) (**b**)

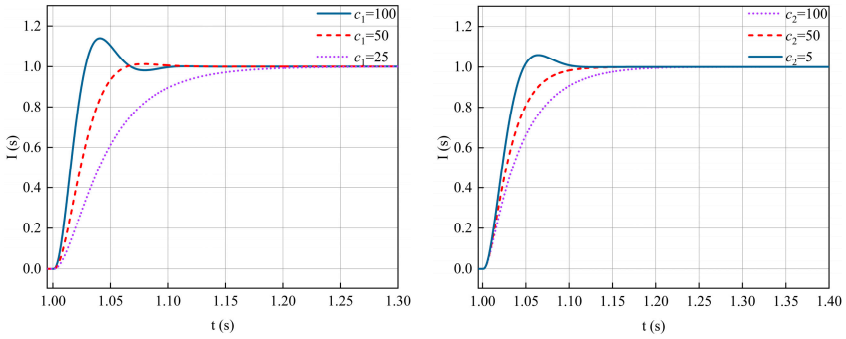
Figure 4. (**a**) Corresponding to different β systems. (**b**) Corresponding to different α systems.

Table 3. Comparison of different β performance parameters.

Parameter	α = 0.01, β = 1	α = 0.01, β = 0.1	α = 0.01, β = 0.01
Overshoot	0.94%	0.12%	0.02%
Rise time	4.3 ms	3.9 ms	3.8 ms
Adjust time (5%)	8.1 ms	7.9 ms	7.5 ms

Table 4. Comparison of different α performance parameters.

Parameter	α = 0.01, β = 0.01	α = 0.1, β = 0.01	α = 1, β = 0.01
Overshoot	0.02%	0.056%	0.062%
Rise time	3.8 ms	5.8 ms	6.2 ms
Adjust time (5%)	7.5 ms	8.5 ms	8.9 ms



(**a**) (**b**)

Figure 5. (**a**) Different c_1 system output. (**b**) Different c_2 system output.

Table 5. Comparison of different c_1 performance parameters.

Parameter	c_1 = 100	c_1 = 50	c_1 = 25
Overshoot	13.99%	1.29%	0.025%
Rise time	18.3 ms	37.1 ms	52.2 ms
Adjust time (5%)	57.9 ms	52.2 ms	128.1 ms

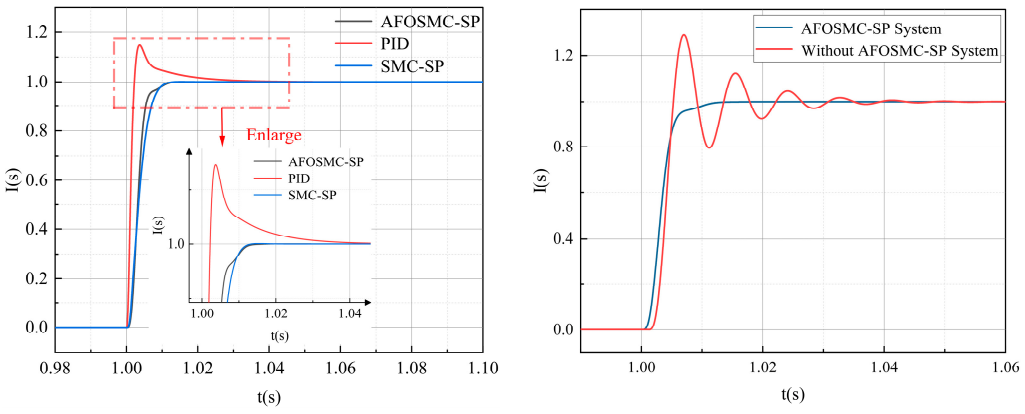
Table 6. Comparison of different c_2 performance parameters.

Parameter	$c_2 = 5$	$c_2 = 50$	$c_2 = 100$
Overshoot	6.01%	0.021%	0.015%
Rise time	30.5 ms	55.3 ms	88.4 ms
Adjust time (5%)	74.2 ms	78.4 ms	124.1 ms

By referring to the tuning and simulation process of an integer-order sliding mode controller, and aiming to reduce overshoot, shorten settling time, and smooth out oscillations, the parameters α, β, c_1, c_2, etc., were selected, as shown in Table 7. The set parameters were brought into the simulation model to verify the validity of the designed adaptive convergence rate, as shown in Figure 6a. Figure 6a presents a comparative simulation study of the AFOSMC-SP, PID control, and conventional SMC-SP strategies. It can be observed that all three control methods are capable of achieving stable tracking; however, significant differences exist in their dynamic performance. The PID controller exhibits a relatively fast response during the rising stage, but it is accompanied by large overshoot and oscillations during the transient process. In contrast, the proposed AFOSMC-SP significantly reduces transient oscillations while maintaining a fast response, resulting in a smoother output trajectory and a more stable steady-state behavior. The simulation results demonstrate that AFOSMC-SP achieves a superior trade-off between dynamic response speed and chattering suppression, thereby exhibiting enhanced robustness and overall control performance.

Table 7. Simulation parameters.

Parameter	Value
α	0.01
β	0.01
ε	0.1
c_1	573
c_2	0.01
N	4
k_0	30
k_1	40



(**a**) (**b**)

Figure 6. (**a**) Comparison of different control strategies. (**b**) Comparison of real FOSMC system and smith predictor-based AFOSMC system.

Figure 6a compares the output characteristics of SMC, PID, and AFOSMC-SP during the system's rising phase and oscillation process. With adaptive sliding mode control, the system exhibits an overshoot of 0.85% and reaches steady state in about 42 ms. In contrast, the improved fractional-order sliding mode control reduces overshoot to 0.025%

and shortens the steady-state time to approximately 8 ms. The PID control strategy shows notably poorer overshoot and response time compared to the other two methods. These results demonstrate that the improved fractional-order sliding mode control effectively suppresses chattering while significantly enhancing system performance, making it highly suitable for control applications demanding high precision, rapid response, and strong robustness. As shown in Table 8, compared to SMC-SP and PID, the fractional-order integral algorithm notably mitigates the chattering issue of SMC and improves the dynamic response of the voice coil motor control system.

Table 8. Comparison of performance parameters.

Parameter	SMC-SP	AFOSMC-SP	PID
Overshoot	0.85%	0.025%	14%
Rise time	35 ms	2 ms	5 ms
Adjust time (5%)	42 ms	8 ms	45 ms

The above simulation results quantitatively confirm that the AFOSMC-SP strategy achieves good comprehensive performance optimization among dynamic response speed, overshoot suppression, and control signal smoothness. SMC-SP typically relies on high and fixed switching gains to ensure fast performance, but this can exacerbate chattering and introduce significant overshoot; although the integral component in PID control contributes to steady-state accuracy, it is prone to overshoot and oscillation during dynamic processes. The AFOSMC-SP strategy proposed in this study is designed through the synergy of fractional-order sliding surface and adaptive convergence law. The non locality and memory properties of fractional-order operators enable the sliding surface to provide softer system dynamics, laying the structural foundation for reducing overshoot and suppressing oscillations. On this basis, by combining the saturation function with the adaptive convergence law of Sigmoid type time-varying gain, sensitive adjustment of the system state is further achieved: when the tracking error is large, the gain is enhanced to accelerate the convergence process; when the error decreases, the gain smoothly attenuates to effectively suppress switching chatter. The combined effect of the two enables the system to adaptively balance response speed and control smoothness during dynamic processes, thereby achieving comprehensive optimization of overshoot, response time, and chattering suppression in simulation.

Meanwhile, the Smith predictor is incorporated to mitigate system delay, as illustrated in Figure 6b. Due to inherent delays, it is observed that while the adaptive sliding mode controller achieves system stabilization within 0.06 s, significant chatters occur during the transient phase, compromising overall stability. In contrast, after integrating the proposed Smith predictor, the system reaches a steady state within 0.02 s with minimal chattering. This demonstrates that the designed controller effectively enhances both robustness and stability.

5.2. Verification of AFOSMC-SP Stability Simulation for Voice Coil Motor

Stabilized control systems are usually affected by one or more types of disturbances in practical applications, such as input disturbances, parameter variations, output disturbances, and internal state disturbances. In this section, the input disturbance (voltage) of a certain amplitude is applied to the system, and the system's output response is analyzed. Then, different types of given signals are input, and the system's tracking output is observed to verify the effectiveness and stability of fractional-order sliding mode control in responding to external disturbances. Additionally, the effects of system parameter changes and the output response of the system under force disturbances are considered.

In the simulation, a pulse disturbance signal with an amplitude of 0.05 and a duration of 1 ms was applied to both the SMC system and the AFOSMC-SP system at t = 1.25 s, and the resulting response is shown in Figure 7a. Overall, both control strategies can effectively suppress the disturbance, quickly return the output to near the set value, and maintain the fluctuation amplitude within a small range, reflecting the system's ability to resist disturbance and stability. Further comparison of the dynamic indicators of the output recovery process shows that traditional SMC has a larger disturbance suppression depth and smaller output fluctuation amplitude, but requires a longer time to recover to steady state; AFOSMC-SP, while effectively suppressing disturbances, can quickly restore system output stability and exhibit better dynamic recovery performance and control efficiency. When the disturbance amplitude is increased, the system's response is shown in Figure 7b. At this point, the oscillation amplitude and overshoot of traditional SMC are significantly higher than those of AFOSMC-SP, indicating that AFOSMC-SP exhibits better robustness in strong disturbance environments. Overall, compared with traditional sliding mode control, FOSMC has a smoother output trajectory, shorter stabilization time, and smaller amplitude fluctuations under the same disturbance conditions.

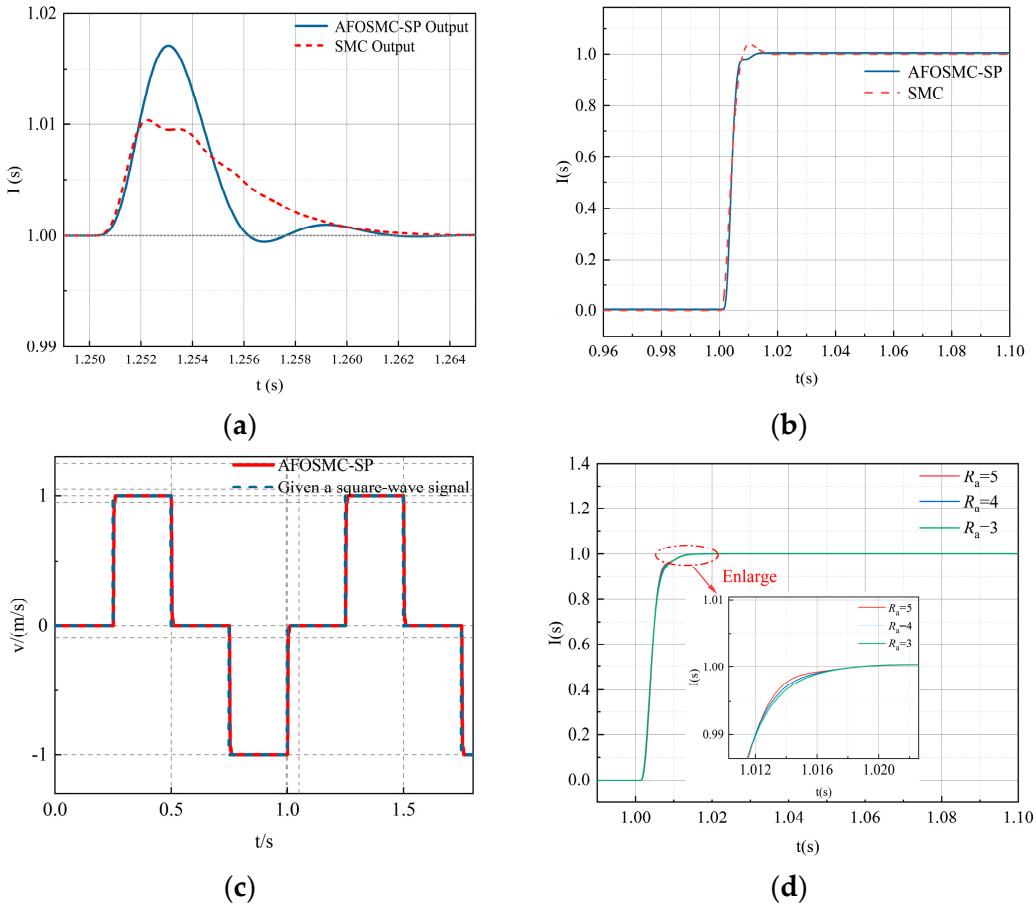


Figure 7. (**a**) Corresponding outputs of the two control systems after a small sudden disturbance. (**b**) Corresponding outputs of the two control systems after a large sudden disturbance. (**c**) The system follows the output when given a square wave signal. (**d**) Comparison of different R_a values.

The square-wave reference signal is introduced to evaluate the controller's ability to handle abrupt and discontinuous reference inputs. As shown in Figure 7c. The system was able to better follow the given square wave signal in its output and respond quickly at the rising and falling edges of the waveform, indicating that the system has good stability and response characteristics.

As shown in Figure 7d, when the system parameter (motor resistance R_a) is disturbed, R_a changes from 3 to 5, and the dynamic characteristics and stability of the system are almost unaffected. This indicates that the system has strong robustness and can maintain stable output characteristics when parameters change.

In summary, both the traditional SMC and AFOSMC-SP have good resistance to disturbances, and the AFOSMC-SP strategy has better performance in the suppression of disturbance amplitude and the time of smooth output, and it can also effectively follow the given in the work, and the stability is more significant.

The estimated disturbance $\hat{d}$ in the disturbance observer can be expressed as follows:

$$\begin{cases} \hat{d}(s) = Q(s)(\frac{ms}{k}I(s) - F(s)) \\ Q(s) = \frac{1}{\delta s+1} \end{cases} \quad (27)$$

Among them, Q (s) is the filter, δ is the time constant, K is the ampere force constant, m is the weight of the rotor, $I(s)$ is the output, and $F(s)$ is the force.

Analyze the stability of the designed disturbance observer. The sufficient conditions for the robust stability of the disturbance observer are as follows:

$$|\Delta(s)| < \left| \frac{1 + C(s)G_0(s)}{Q(s) + C(s)G_0(s)} \right| \quad (28)$$

Among them, $\Delta(s)$ represents the uncertainty of the system model, $C(s)$ is the outer loop controller, and $G_0(s)$ is the nominal model of the system.

The disturbance observer designed by the authors have a low frequency range of $C(s) = 1$ and $Q(s) \approx 1$, therefore, when $s \to 0$, $|\Delta(s)| < 1$ is satisfied, indicating robust stability of the system.

In addition to the AFOSMC-SP design presented above, a disturbance observer is introduced as an auxiliary component in the simulation study to evaluate the robustness of the proposed controller under external force disturbances and model uncertainties. The disturbance estimation of the disturbance observer adopts a low-pass filter Q (s) to preserve low-frequency disturbances and suppress high-frequency noise. To ensure the speed of disturbance estimation while avoiding the amplification of high-frequency noise, the time constant δ in this paper is 0.02, and K is the ampere force constant of the voice coil motor, taken from the parameters of the TMEC series voice coil motor used in this paper, where K = 12.7. Figure 8a compares the output response of the disturbance observer after compensating for small force disturbances with the output response of the system without disturbance observer. Figure 8b compares the output response of the disturbance observer after compensating for larger force disturbances with the output response of the system without a disturbance observer. From the figure, it can be seen that the disturbance observer can effectively compensate for the impact of external force disturbances on the system after being subjected to different magnitudes of disturbance forces, enabling the system to maintain stable output and good dynamic characteristics even under external disturbances.

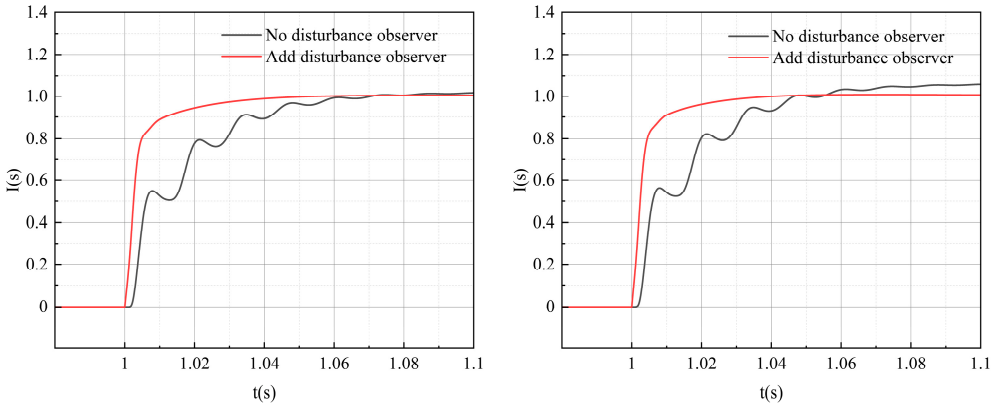


Figure 8. (**a**) The system output characteristics before and after adding disturbance observer when applying small disturbances. (**b**) The system output characteristics before and after adding disturbance observer when applying large disturbances.

6. Conclusions

In this paper, a Smith predictor-based improved adaptive convergence rate fractional-order sliding mode control strategy is proposed for the high-speed positioning control of a voice coil motor (VCM) system with sampling and transmission delays in the current loop. With the coordinated action of delay compensation and adaptive fractional-order sliding mode design, the proposed strategy improves system stability and tracking performance while effectively suppressing chattering and enhancing robustness. The main contributions and conclusions of this study can be summarized as follows:

(1) A unified control framework integrating a Smith predictor and adaptive fractional-order sliding mode control is established. First, a sigmoid-based adaptive reaching law is proposed, enabling the reaching rate to adjust adaptively according to the magnitude of the sliding variable. Meanwhile, the quasi-sliding mode concept is adopted by replacing sgn(s) with sat(s), which further alleviates chattering while ensuring convergence. Second, an improved Oustaloup rational approximation is employed to enhance the approximation accuracy at the endpoints of the target frequency band, resulting in smoother magnitude and phase characteristics with reduced fluctuations. Guidelines for selecting the approximation order are also provided to balance accuracy and implementation complexity. Finally, a Smith predictor is introduced into the current loop to compensate for the equivalent delay, and closed-loop stability is demonstrated based on Lyapunov analysis.

(2) Simulation results indicate that when the controlled plant is a VCM system characterized by high-speed positioning and sampling/transmission delays in the current loop, AFOSMC-SP yields significant performance benefits. Compared with SMC-SP, AFOSMC-SP reduces the system overshoot from 0.85% to 0.025%, shortens the rise time from 35 ms to 2 ms, and decreases the settling time from 42 ms to 8 ms. While improving the dynamic response speed, the system exhibits smaller transient fluctuations and significantly reduced chattering. Moreover, under external disturbances and parameter variations, the system maintains good recovery speed and smooth output behavior, demonstrating strong robustness and stability.

(3) The conclusion of this study is based on simulation analysis and has not yet been experimentally validated using actual hardware platforms. Therefore, further testing is needed to address issues such as real-time computation, nonlinear friction, and robustness to measurement noise in real engineering environments. Future research will focus on the following directions based on experimental verification: Firstly,

although the improved Oustaloup approximation improves the frequency domain fitting accuracy, its increased computational complexity needs to be further optimized in actual processors. Secondly, the fixed boundary layer introduced by the saturation function may affect the convergence speed or steady-state accuracy while suppressing chattering. Subsequently, the time-varying boundary layer design can be studied to better balance the two. Thirdly, for multi-axis or strongly coupled platforms, it is necessary to systematically study the comprehensive design of inter-axis coupling, heterogeneous delay, and multivariable sliding mode surfaces and verify their performance through more comprehensive experiments.

Author Contributions: Investigation, data analysis, establishment of model, simulation and preliminary analysis, writing—original draft preparation, Z.S.; writing—review and editing, X.Y. All authors have read and agreed to the published version of the manuscript.

Funding: This work was supported by the Sichuan University postdoctoral interdisciplinary Innovation Fund 2025; National Natural Science Foundation of Sichuan under Grant 2023NSFSC0826; Project ZR2022QE279 supported by Shandong Provincial Natural Science Foundation.

Institutional Review Board Statement: Not applicable.

Informed Consent Statement: Not applicable.

Data Availability Statement: The original contributions presented in the study are included in the article, further inquiries can be directed to the corresponding author.

Conflicts of Interest: The authors declare no conflicts of interest.

Abbreviations

The following abbreviations are used in this manuscript:

AFOSMC-SP	The adaptive convergence rate fractional-order sliding mode control strategy based on a Smith predictor.
FOSMC	The fractional-order sliding mode control strategy.
SMC-SP	The adaptive sliding mode control strategy based on Smith predictor.
SMC	The sliding mode control strategy.

Appendix A

Definition of the Caputo fractional integral:

$$ {}_aI_t^{-p} = f^{(-p)}(t) = \frac{1}{\Gamma(p)} \int_0^t (t-\tau)^{p-1} f(\tau) d\tau \quad t > 0 \, \mathrm{Re}(p) > 0 $$

Definition of the fractional derivative:

$$ \begin{aligned} {}_aD_t^p f(t) &= {}_aI_t^{n-p} f^{(-p)} {}_aD_t^p f(t) \\ &= \frac{1}{\Gamma(n-p)} \int_0^t (t-\tau)^{n-p-1} f^{(n)}(\tau) d\tau \quad n-1 < p \le n \end{aligned} $$

Oustaloup filter approximation method: By applying the Laplace transform to the fractional-order integral and derivative defined in the Caputo sense, expressions for the fractional-order differential operators s^{p} and $s^{\mathrm{p}-1}$ are obtained:

$$ L\left\{ {}_aD_t^p f(t); s \right\} = s^p(t) F(s) - \sum_{k=0}^{n-1} s^{p-k-1} f^{(k)}(0) \quad n-1 < p \le n $$

References

1. Qiao, Y.; Zhao, T.; Gui, X. Overview of Position Servo Control Technology and Development of Voice Coil Motor. *CES Trans. Electr. Mach. Syst.* **2022**, *6*, 269–278. [CrossRef]
2. Zhao, B.; Shi, W.; Tan, J. Design and Control of a Dual-Stage Actuation Active Vibration Isolation System. *IEEE Access* **2019**, *7*, 134556–134563. [CrossRef]
3. Pan, G.; Zhang, B. Analysis and Modeling Voice-Coil Motor Displacement Change Using an Electrical Simulation Method. In Proceedings of the 2019 International Conference on Electronic Engineering and Informatics (EEI), Nanjing, China, 8–10 November 2019; pp. 60–64.
4. Shewale, M.S.; Razban, A.; Deshmukh, S.P.; Mulik, S.; Zambare, H.B. Design and Experimental Validation of Voice Coil Motor for High Precision Applications. In Proceedings of the 2018 3rd International Conference for Convergence in Technology (I2CT), Pune, India, 6–8 April 2018; pp. 1–6.
5. Wang, Y.; Zhu, Y.; Zhang, X.; Tian, B.; Wang, K.; Liang, J. Anti-disturbance sliding mode-based deadbeat direct torque control for PMSM speed regulation system. *IEEE Trans. Transp. Electrif.* **2021**, *7*, 2705–2714. [CrossRef]
6. Zhang, D.; Qiang, H.; Sun, Y.; Xu, J. Model-Independent Robust Control for Electromagnetic Suspension Systems of Maglev Vehicles. *IEEE Trans. Appl. Supercond.* **2024**, *34*, 3602405. [CrossRef]
7. Xu, G.; Lu, N.; Lv, G. High-Gain Observer-Based Sliding Mode Force Control for the Single-Rod Electrohydraulic Servo Actuator. *IEEE Access* **2019**, *7*, 161849–161857. [CrossRef]
8. Thilagamani, V.; Sakthivel, R.; Aravinth, N.; Ma, Y.K.; Sasirekha, R. Disturbance Observer-Based Robust Control Design for Uncertain Periodic Piecewise Time-Varying Systems with Disturbances. *IEEE Access* **2023**, *11*, 1671–1681. [CrossRef]
9. Guo, J. The Load Frequency Control by Adaptive High Order Sliding Mode Control Strategy. *IEEE Access* **2022**, *10*, 25392–25399. [CrossRef]
10. Shi, S.; Gu, J.; Xu, S.; Min, H. Globally Fixed-Time High-Order Sliding Mode Control for New Sliding Mode Systems Subject to Mismatched Terms and Its Application. *IEEE Trans. Ind. Electron.* **2020**, *67*, 10776–10786. [CrossRef]
11. Bartoszewicz, A. Discrete-time quasi-sliding-mode control strategies. *IEEE Trans. Ind. Electron.* **1998**, *45*, 633–637. [CrossRef]
12. Fan, W.; Yan, P. A Novel Disturbance Observer Design Method for Time Delay Systems with Application to Nano Manipulations. In Proceedings of the International Conference on Advanced Mechatronic Systems (ICAMechS), Zhengzhou, China, 30 August–2 September 2018; pp. 353–358.
13. Levant, A. Quasi-continuous high-order sliding-mode controllers. *IEEE Trans. Autom. Control* **2005**, *50*, 1812–1816. [CrossRef]
14. Bian, F.; Chien, Y.-R. PMSM Speed Control Based on Improved Adaptive Fractional-Order Sliding Mode Control. *Symmetry* **2025**, *17*, 736. [CrossRef]
15. Kumar, N.; Saha, T.K.; Dey, J. Design and analysis of a double band hysteresis SMC for cascaded inverter-based PV system. In Proceedings of the IEEE Region 10 Conference (TENCON), Singapore, 22–25 November 2016; pp. 898–902.
16. Huang, J.C.; Shi, X.X.; Li, H.S.; Shi, Y.W. Fractional order integral sliding mode control for permanent magnet synchronous motor speed control system. *J. Jilin Univ.* **2014**, *44*, 1736–1742.
17. Chen, Y.; Bu, W.; Qiao, Y. Research on the Speed Sliding Mode Observation Method of a Bearingless Induction Motor. *Energies* **2021**, *14*, 864. [CrossRef]
18. Zhao, X.M.; Wang, C.; Jing, H.Y. Adaptive fractional order sliding mode control of permanent magnet synchronous motor based on NDO. *China Mech. Eng.* **2023**, *34*, 1093–1099+1119.
19. Zhang, B.T.; Pi, Y.G. Permanent magnet synchronous motor control based on fuzzy fractional order sliding mode contro. *J. South China Univ. Technol.* **2012**, *40*, 126–130.
20. Wang, Y.; Gu, L.; Xu, Y.; Cao, X. Practical Tracking Control of Robot Manipulators with Continuous Fractional-Order Nonsingular Terminal Sliding Mode. *IEEE Trans. Ind. Electron.* **2016**, *63*, 6194–6204. [CrossRef]
21. Feng, D.-M.; Pan, F.; Han, R.-C. Improved self-adaptive Smith predictive control scheme for time-delay system. In Proceedings of the International Conference on Machine Learning and Cybernetics, Beijing, China, 4–5 November 2002; Volume 1, pp. 463–466.
22. Fliess, M.; Marquez, R.; Mounier, H. An extension of predictive control, PID regulators and Smith predictors to some linear delay systems. *Int. J. Control* **2002**, *75*, 728–743. [CrossRef]
23. Jesus, I.S.; Barbosa, R.S. Smith-fuzzy fractional control of systems with time delay. *AEU Int. J. Electron. Commun.* **2017**, *78*, 54–63. [CrossRef]
24. Wang, C.; Liang, M.; Chai, Y. Adaptive Control of a Class of Incommensurate Fractional Order Nonlinear Systems with Input Dead-Zone. *IEEE Access* **2019**, *7*, 153710–153723. [CrossRef]

Disclaimer/Publisher's Note: The statements, opinions and data contained in all publications are solely those of the individual author(s) and contributor(s) and not of MDPI and/or the editor(s). MDPI and/or the editor(s) disclaim responsibility for any injury to people or property resulting from any ideas, methods, instructions or products referred to in the content.